Postprint version of the paper published in Nanomedicine
Nanomedicine: Nanotechnology, Biology and Medicine
Volume 11, Issue 3, April 2015, Pages 731-739,
https://doi.org/10.1016/j.nano.2014.11.002

Negligible particle-specific toxicity mechanism of silver nanoparticles: The role of Ag^+ ion release in the cytosol

Valeria De Matteis, Maria Ada Malvindi, Antonio Galeone, Virgilio Brunetti, , Elisa De Luca, Sachin Kote, Prakash Kshirsagar,Stefania Sabella, Giuseppe Bardi, Pier Paolo Pompa*

Istituto Italiano di Tecnologia, Center for Bio-Molecular Nanotechnologies@Unile, Arnesano (Lecce), Italy

: pierpaolo.pompa@iit.it

Abstract

Toxicity of silver nanoparticles (AgNPs) is supported by many observations in literature, but no mechanism details have been proved yet. Here we confirm and quantify the toxic potential of fully characterized AgNPs in HeLa and A549 cells. Notably, through a specific fluorescent probe, we demonstrate the intracellular release of Ag^+ ions in living cells after nanoparticle internalization, showing that in-situ particle degradation is promoted by the acidic lysosomal environment. The activation of metallothioneins in response to AgNPs and the possibility to reverse the main toxic pathway by Ag^+ chelating agents demonstrate a cause/effect relationship between ions and cell death. We propose that endocytosed AgNPs are degraded in the lysosomes and the release of Ag^+ ions in the cytosol induces cell damages, while ions released in the cell culture medium play a negligible effect. These findings will be useful to develop safer-by-design nanoparticles and proper regulatory guidelines of AgNPs.

.

Key words: Silver; Nanoparticles; Toxicity; Ion release

The advancement in the production and characterization of several nanomaterials in the last decade allowed their application in many different fields, including biomedicine.[1] Among nanomaterials, silver nanoparticles (AgNPs) have found application in a wide range of medical products, owing to their peculiar physico-chemical features, such as potent and broad-spectrum antibacterial activity.[2,3] Indeed, AgNPs are extensively employed in food[4] and health[5] sectors to reduce the contamination of micro-organisms. New textile products for sport activity are nowadays under production and commercialization increasing their environmental impact.[6] Furthermore, their optical/electronic properties allow their employment as diagnostic bio-sensing and imaging probes[7] or in conductive inks,[8,9] significantly increasing their range of applications. The growing relevance of production and market request, therefore, call for deep knowledge of environmental discharge and AgNPs' toxicological impact on human health. Cell death induced by AgNPs, as well as gene expression and release of inflammatory cytokines following their administration, has been shown in cells *in vitro*[10-12] and *in vivo*, such as in mammalians,[13,14] nematodes,[15,16] fishes[17,18] and artropodes.[19] Despite a commonly recognized toxicity[20] and a role of nanoparticle size and chemistry,[21,22] the underlying cellular and molecular mechanisms still remain unclear.[23] In particular, the contribution of ions release from the nanoparticle to the AgNP-induced cell death is still debated. While some researchers identified a particle-related oxidative stress-dependent toxicity,[24] others suggest that both AgNPs and the release of silver ions contribute to the cell death.[25,26] An intriguing speculation that endocytosed AgNPs would be ionized inside the cell and trigger toxicity, through a Trojan-horse type mechanism, was supposed after the observation that AgNPs were found in the cytosol of activated macrophages but not inside dead cells.[26] Nevertheless, no direct Ag^+ ions release inside the cell, following AgNPs exposure, has been shown to date. Moreover, the evaluation of AgNPs activity on cells was sometimes compromised by the low NPs quality and/or their incomplete physico/chemical characterization, which contributed to the diverse observations in literature. To assess the mechanism of toxicity

induced by AgNPs, we exposed cell lines derived from two different tissues, namely HeLa and epithelial A549 cells, to fully characterized and highly monodisperse 20 nm AgNPs. A comprehensive AgNP impact on cell viability was evaluated by metabolic activity, reactive oxygen species (ROS) production, necrotic and apoptotic triggered pathways, as well as genotoxicity and cell cycle impairment. This significant amount of cellular information together with the analysis of particle degradation *in situ* and intracellular release of silver ions prompts us to modeling a feasible mechanism for AgNP-induced toxicity. We show that the observed toxicity in AgNP-treated cells is mainly caused by a heavy metal type mechanism following nanoparticle degradation in the acidic compartments of the cells and the subsequent extrusion of Ag^+ ions in the cytosol. The activation of metallothioneins and demonstration of cell protection by Ag^+ chelating agents proved our hypothesis.

Methods

Synthesis of silver nanoparticles (AgNPs)

The synthesis of AgNPs was performed according to a literature procedure with some modifications.[27] We prepared an aqueous solution of tri-sodium citrate (final concentration 1.36 mM) containing 2.9 μM tannic acid. The solution was heated at 60 °C, and a solution of $AgNO_3$ (0.592 mM final concentration) was added while stirring. When the mix became yellow, it was boiled for 30 min, then cooled at room temperature and stored in the dark at 4 °C.

Cell culture

HeLa cells (human cervix carcinoma, ICLC, HTL95023) and A549 cells (human lung carcinoma, HTL03001) were routinely cultivated in high glucose DMEM with 50 μM glutamine, supplemented with 10% FBS, 100 U/mL penicillin and 100 mg/mL streptomycin. Cells were incubated in a humidified controlled atmosphere with a 95% to 5% ratio of air/CO_2, at 37 °C. Medium was changed every 3 days.

WST-8 assay

HeLa and A549 cells were seeded in 96 well microplates at a density of 5000 cells/well at final volume of 50 μl and incubated for 24 h in a humidified atmosphere at 37 °C and 5% CO_2 to obtain a subconfluent monolayer (60-70% of confluence). AgNPs were dispersed in cell culture medium to attain stock solutions and added at the single well obtaining a final AgNPs concentrations of 0.06, 0.3, 0.6 nM in a final volume of 100 μl for each well. WST-8 (Sigma) assay were performed following the procedure previously described in Malvindi et al.[28] Data were expressed as mean ± SD. Differences in cell proliferation (WST-8) between cells treated with AgNPs and the control were considered statistically significant performing a Student *t* test with a *P*-value b 0.05.

LDH assay

HeLa and A549 cells were seeded in black 96 well microplates (Constar) and treated with AgNPs at concentrations of 0.06, 0.3, and 0.6 nM. After 48 and 96 h of cell–AgNP interaction, the lactate dehydrogenase (LDH) leakage assay was performed onto microplates by applying the CytoTox-ONE Homogeneous Membrane Integrity Assay reagent (Promega), following the manufacturer's instructions.[29] Positive controls consisted in the treatment of such cells with 0.9% Triton X-100. Data were expressed as mean ± SD. Differences in LDH leakage between cells treated with AgNPs and controls were considered statistically significant performing a Student *t* test with a *P*-value b 0.05.

DCF assay

HeLa and A549 cells were seeded in 96-well microplates and treated with AgNPs at a final concentration of 0.06, 0.3 and 0.6 nM. After 48 and 96 h of cell–NP interaction the DCF-DA (2′,7′-dichlorofluorescein diacetate, Sigma) assay was performed onto microplates following the procedure reported by Malvindi et al.[28] Data were expressed as mean ± SD. Differences in ROS generation between cells treated with AgNPs and controls were considered statistically significant performing a Student *t* test with a *P*-value b 0.05.

JC-1 assay

HeLa and A549 cells were seeded in black 96 well microplates (Constar) and treated with AgNPs at concentrations of 0.06, 0.3 and 0.6 nM. After 48 and 96 h of cell–NP interaction, the mitochondrial membrane potential assay (Molecular probes JC-1, Invitrogen) was performed onto microplates, following the manufacturer's instructions by using Fluo Star Optima (BMG LABTECH) microplates reader. After removing the medium, the cells in the plates were washed with PBS buffer and then incubated with 2.5 μg/mL JC-1 in the loading medium (DMEM 1% FBS). After loading medium was removed, the cells were washed and incubated with PBS buffer and the fluorescence of the cells from each well was measured and recorded. Results are normalized with respect to negative controls (expressed as 100%). As a positive control, cells were incubated with 100 μM valinomycin. Data were expressed as mean ± SD. The difference between cells treated with AgNPs and controls was considered statistically significant performing a Student *t* test with a *P*-value b 0.05.

Caspase-3 activation

Caspase-3 activity was detected by using CASP-3-C (Sigma). HeLa and A549 cells (1×10^7) were collected after 24 h of incubation in the presence of AgNPs at concentration values of 0.6 nM. After treatments, cells were lysed on ice with 50 mL of lysis buffer for 10 min. Afterwards, 50 mL of reaction buffer containing dithiothreitol (DTT) and 5 mL of caspase-3 substrate solution (acetyl-Asp-Glu-Val-Asp p-nitroanilide [Ac-DEVD-pNA]) were added. The concentration of the released pNA from the substrate was calculated by measuring absorbance at 405 nm by using Fluo Star Optima. Data were collected by Control Software and elaborated with MARS Data Analysis Software (BMG LABTECH). The caspase 3 activity of each sample was expressed in μmol of pNA released per min per ml of cell lysate; the percentage of caspase 3 activity was calculated using the following equation: (activity treated sample/activity

control) × 100. Data were expressed as mean ± SD. The reproducibility of the results was guaranteed by performing four independent biological replicates.

Cell cycle analysis

Cell cycle analysis was carried out by staining the DNA with propidium iodide (PI) followed by flow cytometric measurement. Approximately 10^6 HeLa cells were placed in 100 mm tissue culture dish. The HeLa cells were treated with AgNPs 0.6 nM for 3 h. After 3 h the AgNPs were removed and the cells were reincubated at 37 °C for 48 and 96 h. The cells were centrifuged at 300 g for 5 min and washed with PBS. HeLa were slowly resuspended with 1 mL of ice cold ethanol (70%) and incubated for 3 h at − 20 °C. Before flow cytometry analysis, 200 μL of fixed cells was placed in a new tube and centrifuged at 300 g for 5 min and washed with PBS. Cells were stained with PI and incubated for 30 min at room temperature in the dark. Flow cytometry analysis was performed using Muse Cell Analyzer (Millipore).

Determination of the intracellular uptake of AgNPs and Ag^+ ions

To estimate the intracellular nanoparticles uptake, 10^5 cells were seeded in 1 mL of medium in each well (3.5 cm in diameter) of a 6-well plate. After 24 h of incubation at 37 °C, the medium was replaced with fresh medium containing the nanoparticles at a concentration of 0.6 nM. After 48 and 96 h of incubation at 37 °C, the medium was removed; the cells were washed three times with PBS (pH 7.4), trypsinized, and counted using a cell-counting chamber. Then, the cell suspensions were digested using 1 mL of concentrated HNO_3 10% (v/v) and the intracellular Ag concentration was measured by means of elemental analysis and normalized to the number of cells. The same procedure was employed to evaluate the uptake of Ag^+ ions (we used 100 μM of $AgNO_3$ corresponding to 0.6 nM of AgNPs).

Confocal microscopy imaging

The fluorescent chemosensor RC-1 was kindly provided by Dr. Mingming Hu and Dr. Xiaojun Peng (State Key Laboratory of Fine Chemicals, Dalian University of Technology, China). For the analysis of the intracellular release of Ag^+ ions with the RC-1 probe, A549 cells were treated for 3 h with 0.6 nM AgNPs and washed with PBS. Cells were then loaded with the fluorescent probe RC-1 (1 μM) for 20 min at 37 °C in 5% CO_2, subsequently washed 3 times with PBS to remove the excess of the probe, and analyzed by confocal microscopy. The images were recorded after 0, 24, 48 and 96 h with a Confocal Microscope Leica TCS SP8 using a 40 × oil immersion objective (PL APO CS2 40 ×/1.30 OIL). In order to further quantify the fluorescence, image files were reanalyzed with ImageJ software. Histograms of red (RC-1) positive pixel were analyzed. We used the tool ImageJ/Analyze/Histogram/List, followed by the sum of the counted pixels. The positive pixels at lower intensity (5% of the total pixels) were excluded in order to avoid background noise. To evaluate the statistical significance of the Ag^+ ion intracellular release over time, the *t* test on the results from the collected pictures at different time points (24 h, 48 h, 96 h) vs. control (0 h) was performed.

For the immunofluorescence analysis of MT expression, the images were recorded with the same confocal microscope using a 488 nm excitation wavelength for FITC signal detection, and a 405 nm wavelength for Hoechst staining.

Measurements of NP ion release

The evaluation of NP ion release was performed at 37 °C both in acidic conditions (sodium citrate buffer, pH 4.5), an acidic medium mimicking the lysosomal environment, and in neutral conditions (ultrapure water and DMEM, pH 7). The citrate buffer was prepared by mixing appropriate volumes of 20 mM aqueous solutions of citric acid and sodium citrate monobasic to achieve the final desired pH. The ion release was analyzed at 24, 48, 72 and 96 h. At each time point, the NPs were separated from the rest of solution through centrifugation at 13000 rpm for 1 h. Solutions were collected and digested by the addition of a solution of HNO_3 10% (v/v), and the amount of free ions was measured by ICP-AES (Inductively Coupled Plasma Atomic Emission Spectrometer).

Comet assay (single cell gel electrophoresis)

HeLa and A549 cells were exposed to 0.6 nM AgNPs for 48 h, at density of 5×10^4 in each well of 12-well plates in a volume of 1.5 mL. After treatments, cells were centrifuged and suspended in 10 μl of PBS at concentration of 1000 cells/μl. The cell pellets were mixed with 75 μl of 0.75% low-melting-point agarose (LMA) and then layered onto microscope slides precoated with 1% normal melting agarose (NMA) and dried at room temperature. Subsequently, the slides were immersed in an alkaline solution (300 mM NaOH, 1 mM Na_2EDTA, pH 13) for 20 min to allow for unwinding of the DNA. The electrophoresis was carried out in the same buffer for 25 min at 25 V and 300 mA (0.73 V/cm). After electrophoresis, cellular DNA was neutralized by successive incubations in a neutralized solution (0.4 M Tris–HCl, pH 7.5) for 5 min at room temperature. The slides were stained with 80 μl SYBR Green I (Invitrogen). Comets derived from single cells were photographed under a Nikon Eclipse Ti fluorescence microscope, and head intensity and tail length of each comets were quantified using Comet IV program (Perceptive Instruments).

Antibodies

Mouse monoclonal anti-metallothionein antibody [UC1MT] (ab12228, Abcam), mouse monoclonal anti-GAPDH antibody (ab9484, Abcam), goat anti-mouse IgG FITC-conjugated antibody (sc-2010, Santa Cruz Biotechnology), and goat anti-mouse IgG (H + L)-HRP conjugate (170-6516, Bio-Rad).

Immunofluorescence microscopy

HeLa cells were plated on Millicell® EZ slides 8-well (Millipore) in DMEM supplemented with 10% fetal calf serum (FCS) and left untreated or treated with AgNPs (20 nM) in DMEM at 37 °C for 3 h. Cells were fixed with 4% paraformaldehyde in PBS for 10 min, permeabilized with PBS 0.5% Triton X-100 for 1 min, and treated with PBS 1% BSA to block unspecific binding sites. Immunofluorescence microscopy was performed using the primary antibody followed by incubation

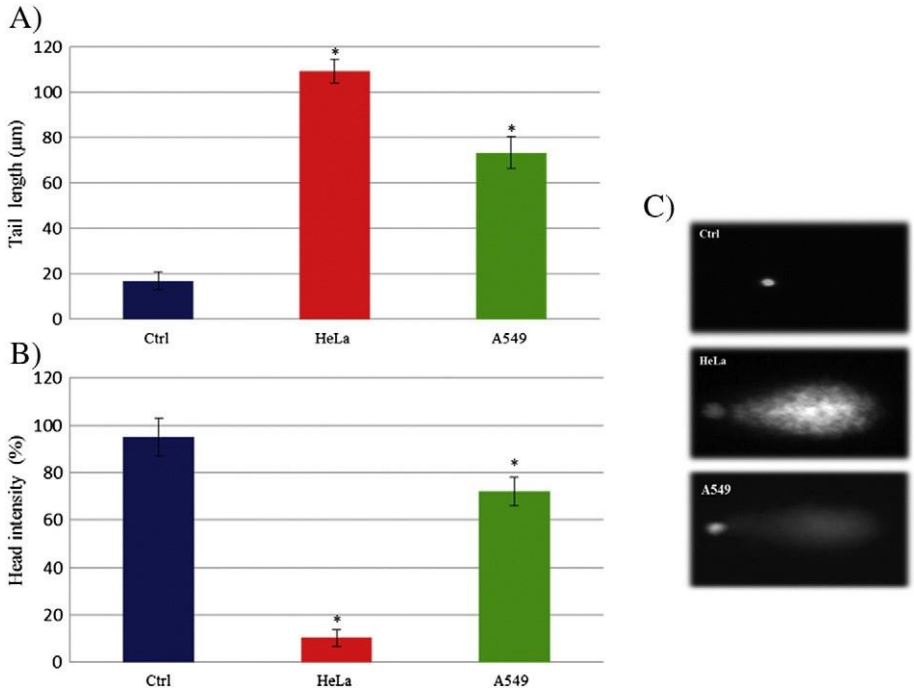

Figure 1. Effect of AgNPs on DNA damage determined by comet assay. HeLa and A549 cells were treated with 0.6 nM of NPs for 48 h. DNA damage was evaluated by (A) tail length (µm) and (B) head intensity (%). Values shown are means from 100 randomly selected comet images of each sample. As a positive control (P) cells were incubated with 500 µM H_2O_2. (C) Representative images of AgNP effect on DNA damage in the two cells lines. Data are reported as mean ± SD from three independent experiments; *P b 0.05 compared with control (n = 3).

with the FITC-conjugated secondary antibody. Nuclei were stained with Hoechst (Sigma).

Western blotting analysis

HeLa cells were cultured in complete medium and treated with AgNPs (20 nM) in serum-free medium for 3 h. Cells were washed with PBS, and the complete medium was added to the culture and left up to protein extraction. Cells were lysed with RIPA lysis buffer (R0278, Sigma) with protease inhibitors (P8340, Sigma) and phosphatases inhibitor cocktails (P2850, Sigma). The extracts were then clarified by centrifugation at 14000 rpm for 10 min. Further proteins were subjected to 2D clean up kit (80-6484-51, GE) and purified proteins quantified by using 2D Quant kit (80-6483-56, GE) according to the manufacturer's instruction. Equal amounts of total proteins (~ 30 µg) were separated by 4-20% gradient mini precast TGX gel (456–1093, Bio-Rad) and electroblotted onto PVDF membrane (0.2 µm, 162-0177, Bio-Rad). The blots were blocked with chemiluminescent blocker (Millipore) for 1 h at room temperature. The membrane was incubated with primary antibody overnight at 4 °C and subsequently with HRP-conjugated secondary antibody (170-6516, Bio-Rad) for 1 h at RT. Proteins were visualized according to the manufacturer's instruction by an enhanced chemiluminescence (ECL) detection system (Bio-Rad) with Typhoon Trio (GE). Protein band intensity was quantified by using 1D image Quant (GE) program.

Effect of 2,3 dithiopropanol (BAL) on cell toxicity

To study the effect of silver chelator on ROS generation, cells were incubated with or without BAL (1 µM) and a suspension of AgNPs (0.06 nM). After 48 h of incubation at 37 °C, the medium was removed, the cells were washed three times with PBS (pH 7.4), and the ROS generation was estimated by DCFH-DA assay.

Results

Monodispersed and stable AgNPs were synthesized in our laboratory. Their physico-chemical characterization was carried out both in water and in cell culture medium, using a panel of different techniques, namely TEM, DLS, NTA, Z-Potential, UV–vis. TEM analyses revealed that AgNPs have a good spherical morphology with a size of 20 ± 2 nm (Figure S1, *A*). Monodispersion was confirmed in solution by DLS and NTA, both showing a peak corresponding to 20 nm (Figure S1, *B* and *C*). The Z-potential of AgNPs was − 16 mV (Figure S1, *D*), while a sharp plasmon peak at c.a. 400 nm (Figure S1, *E*) was indicative of highly monodispersed NPs. In DMEM culture medium, we observed an increase in AgNPs size up to ~ 70 nm (Figure S2, *A* and *B*), and the NP surface charge became more negative (− 28 mV) (Figure S2, *C*), most likely due to the protein corona formation.[30,31] Furthermore, the evaluation of broader and red-shifted absorption peak in the UV–vis spectrum suggests the formation of some NP aggregates (Figure S2, *D*).

In order to evaluate and quantify the toxic effects of AgNPs, we tested many different parameters in HeLa and A549 cell lines. Treatment with AgNPs induced a clear dose-dependent viability reduction (Figure S3) in both cell lines, as measured by the WST-8 assay. Cell membrane damage was revealed by LDH release giving us information on, at least, one mechanism for cell

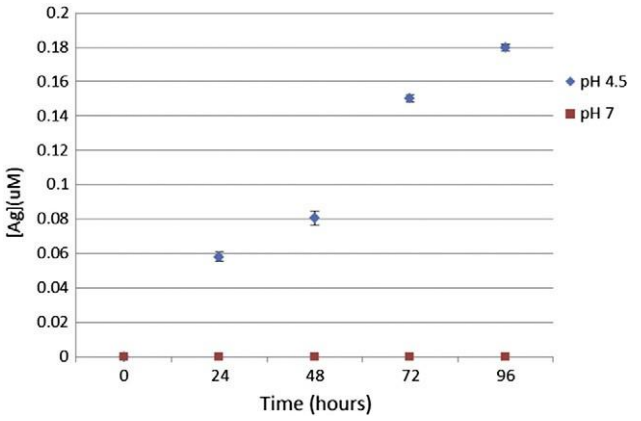

Figure 2. Effects of time and pH on silver ions release from AgNPs (100 pM). NP degradation was evaluated both at pH 4.5 and 7 up to 96 h. NP degradation in neutral conditions was analyzed also in culture medium, finding the same behavior observed in water.

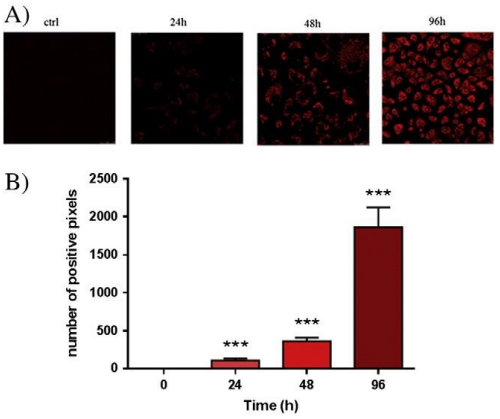

Figure 3. Presence of Ag^+ ions in A549 cells after treatment with AgNPs. (A) Representative confocal fluorescence images of living A549 cells treated with 0.6 nM AgNPs. After 3 h NPs were removed by washing with PBS and cells loaded with the Ag^+ ion specific fluorescent probe (1 μM) for 20 min. The images were recorded after 24, 48 and 96 h. Ctrl represents cells treated with 1 μM probe. The Ag ions released in cells upon the NP degradation are detectable through the increase of the probe fluorescence over time. (B) Histograms of fluorescent positive pixel were analyzed. The positive pixels at lower intensity (5% of the total pixels) were excluded in order to avoid background noise. The intensity was measured and quantified in all the pictures. Unpaired t-test (***P value b 0.001).

death (Figure S4). In general, we observed that A549 cells were more resistant than HeLa to the treatment with AgNPs (see also Discussion section).

The administration of AgNPs to cells has been already shown to promote ROS- and JNK-dependent apoptotic pathways and alterations of the mitochondrial membrane potential (MMP),[32,33] as well as cytotoxicity, DNA damage[34] and cell cycle arrest following caspase activation.[35] We confirmed the NP ability to induce oxidative stress by means of the DCFH-DA assay. The generation of ROS in treated cells of both types was significantly different from the controls, even at the lowest nanoparticle concentration tested (0.06 nM) (Figure S5, *A*). The fluorescence intensity increase of the specific ROS reporter was also clearly observed by confocal microscopy in treated cells, as a function of AgNPs concentration (Figure S5, *B*).

Perturbations of the mitochondrial membrane potential (MMP), assessed by JC-1 assay, resulted to be dose dependent and particularly evident at high concentrations (Figure S6). We also observed significant genotoxicity of AgNPs. Using the comet assay, we found high level of DNA damage after AgNP administration, both in terms of tail length and DNA percentage in the head (Figure 1, *A* and *B*), showing the typical comet morphology (Figure 1, *C*). DNA damages begin a signal cascade that activates cell-cycle checkpoints and DNA-repair mechanisms, which subsequently induce the arrest of the cell cycle progression.[36,37] As shown in other types of human and mouse cells, AgNPs induced cell cycle arrest at S/G2/M phase of cell cycle.[35-38] Accumulation of cells in G2 and M phase with a decrease in the corresponding G1 and S populations in a time-dependent manner (Figure S7) was confirmed in our laboratory in AgNPs-treated HeLa and A549 cells by flow cytometry.

Caspase-3 plays a key role in several apoptotic mechanisms[39] and it is frequently used as a marker of the entry point into the apoptotic signaling pathway.[40] Figure S8 shows the increase of caspase-3 levels after 24 h of NP treatment, proving that caspase-3 triggered apoptosis took place in presence of AgNPs.

In order to quantify the amount of AgNPs taken up per cell, we performed elemental analysis by inductively coupled plasma atomic emission spectroscopy (ICP-AES). Experimental data confirmed the presence of Ag in both cell lines, with time-dependent internalization efficiency (Figure S9). A549 cells showed a larger nanoparticle uptake. Intriguingly, HeLa cells were more susceptible to AgNP induced toxicity, whereas the epithelial cell line A549 confirmed its ability to internalize more NPs.

We investigated whether the intracellular release of silver ions was necessary to the AgNP-induced toxicity. Most of silver NPs are internalized by endocytosis and move into the lysosomes, as shown by TEM and confocal microscopy imaging (Figure S10). NPs can undergo a degradation process in these acidic compartments, releasing ions that cross the organelle membrane spreading into the cytosol. To mimic the impact of the acidic lysosomal conditions or cell culture medium on AgNP stability and ion release, we analyzed their degradation at pH 4.5 and 7, respectively. The kinetics of the NP dissolution was monitored by elemental analysis, resulting significantly dependent on the pH. AgNP released ions at pH 4.5 increased over time. On the contrary, in water or cell culture medium at neutral pH, no appreciable ion release was observed (Figure 2). These data do not mean that at neutral pH there is zero release of Ag^+ ions from the AgNPs, but rather that the ion release is strongly promoted by the acidic environment (in Figure 2 we used a low initial particles concentration, i.e. 100 pM; the dissolution behavior at a significantly higher concentration, i.e. 10 nM, is reported in Figure S11; typically, the dissolution of our AgNPs after 96 h ranged from ca. 1-3% of the total nanoparticle mass).

To provide evidence that the release of Ag^+ ions occurs in cells after AgNP administration, we took advantage of the

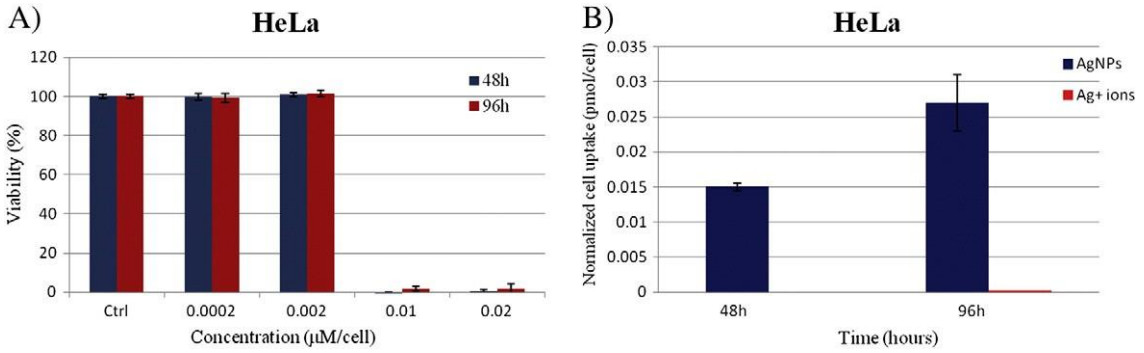

Figure 4. (A) Viability assay (WST8) of HeLa cells after 48 and 96 h exposure to increasing doses of silver ions: 0.0002, 0.002, 0.01, and 0.02 μM/cell, corresponding to 0.1, 1, 5, 10 μg/mL. Percent viability of ion-treated cells was expressed relative to non-treated control cells. Data are reported as mean ± SD from three independent experiments. (B) Internalization data for HeLa cells expressed as amount of internalized silver ions (determined by ICP-AES) per cell after 48 and 96 h of ions incubation. Internalization data of AgNPs (incubated at the same silver concentration, 1 μg/ml Ag) are shown for comparison.

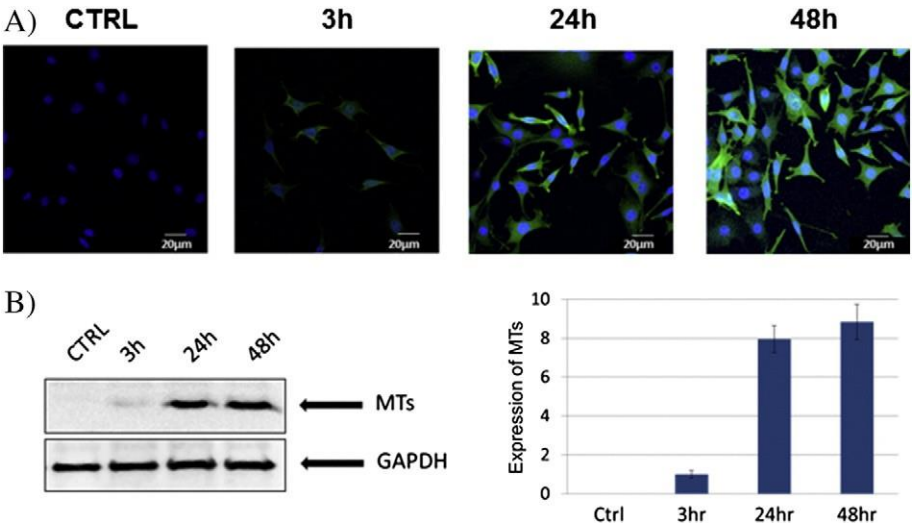

Figure 5. (A) Representative immunofluorescence of metallothionein expression in HeLa cells treated for 3 h with AgNPs and fixed immediately after the treatment (3 h) or 24 h and 48 h after the treatment. Nuclei are visualized by DAPI staining and metallothioneins with a primary anti-metallothioneins antibody coupled with a FITC-labeled secondary antibody. The expression of metallothioneins in cells treated with AgNPs increases over time. Ctrl represents cells without AgNPs treatment. (B) Western blot analysis and densitometric analysis of metallothionein (MT) expression in HeLa cells treated with AgNPs at 24 and 48 h.

recently developed enhanced fluorescent chemosensor RC-1 that can selectively detect Ag^+ in living cells.[41] The fluorescence of the probe was evaluated in living A549 cells treated with AgNPs and followed for 96 h by confocal microscopy. As shown in Figure 3, *A*, the presence of silver ions in the cytosol was emphasized by the significant increase in RC-1 fluorescence after 24 h and the progressive increase over the observation time. Figure 3, *B* shows the number of the red fluorescence (RC-1) positive pixels in the different pictures, revealing statistical significance at all the time points analyzed. This is in agreement with the hypothesis of AgNP degradation in the acidic compartments of living cells. The fluorescent probe was distributed in cytoplasm, organelles and nuclei, indicating that the silver ions diffused in whole cell, as already reported in other systems.[42] This revealed for the first time the kinetics of dissolution of AgNPs in living cells, and demonstrated that AgNP toxicity is strictly dependent on the release of silver ions from AgNPs in the cell (see also below).

The possibility that the cytotoxic effects described so far in the present report could be also due to the entrance of silver ions from the external medium is remote. We evaluated cell viability after treatment with silver ions dispersed in culture medium at concentrations ranging from 0.1 to 10 μg/ml, the latter corresponding to the theoretical complete dissolution of 0.6 nM AgNPs. Consistent with previous reports,[43] the viability of HeLa cells was not influenced by extracellular Ag^+ ions up to 1 μg/ml (Figure 4, *A*), namely Ag^+ concentration much higher than that released in the medium even by the highest NP dose used in our experiments. This is most likely because of the very low amount of Ag^+ ions internalized by cells from the extracellular medium (Figure 4, *B*). At ion concentrations ≥ 5 μg/ml, we observed almost immediate cell death, due to Ag^+ ions-induced impairment of cell membrane permeability to ions K^+ and Na^+.[44]

Metallothioneins (MTs) are small proteins localized in the Golgi apparatus and involved in the regulation of metals. Roughly 30% of their amino acidic content is represented by cysteine

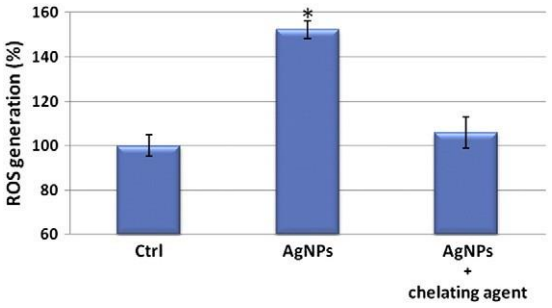

Figure 6. Effect of specific ion chelator BAL (2,3 dithiopropanol) on ROS generation (probed by DCFH-DA assay) induced by AgNPs (0.06 nM) on HeLa cells. HeLa cells were pretreated for 30 min with/without 1 μM BAL and then exposed to the AgNPs for 48 h. It is evident that the pretreatment with the chelating agent suppresses almost totally the toxicity of the NPs. CTRL represents the negative control; values are means + SD. Differences between treated samples and controls (n = 8) were considered statistically significant for *P b 0.05, non-significant for P N 0.05.

residues, conferring to the MTs high affinity for heavy metals through the thiol groups.[45] Their expression is enhanced when the intracellular concentration of heavy metals is increased, facilitating metal detoxification and protection from free radicals.[46,47] Specifically, up-regulation of MTs has been observed in response to the exposure of astrocytes to AgNPs.[47] We monitored for 48 h their expression in HeLa cells treated with the nanoparticles by immunofluorescence and Western blot analysis. Both techniques revealed that AgNP-treated cells strongly upregulated the expression of MTs, and this phenomenon progressively increased over time (Figure 5, *A* and *B*). This suggests a heavy metals type toxicity mechanism of AgNPs.

Furthermore, to have the fundamental proof of Ag^+ ions as the principal mediators of the toxic effect, we demonstrated that it is possible to protect the cells from the NP injury, through the administration of metal ion chelating agents (Figure 6). Interestingly, we found that ROS generation following cell internalization of AgNPs was completely abrogated in presence of the ion chelator BAL (2,3 dithiopropanol).

Discussion

Albeit the agreement among several authors about the toxic potential of silver nanomaterials,[48,49] the responsibility of AgNPs or Ag^+ ions in the mechanism leading to cell damage and death was still not understood. In the present manuscript we demonstrated experimental proofs of negligible effect of particles and a deleterious effect of Ag^+ ions.

One of the main toxicity pathways is triggered by the presence of intracellular metal ions in excess that stimulate an increase of ROS, produced by cellular oxygen metabolism.[50,51] This phenomenon, known as "oxidative stress" is positively used by phagocytes to destroy entrapped pathogens (e.g., bacteria). On the other hand, uncontrolled ROS production can lead to serious cellular injuries,[52] such as DNA damage[53] and of mitochondria-involved apoptotic cell death.[54] In eukaryotic cells, ROS levels are physiologically controlled by antioxidative enzymes and low molecular weight antioxidants (e.g., glutathione).[51-54] The presence of silver ions in the cytosol unbalances the equilibrium increasing the ROS with deleterious effects. We carefully investigated this pathway in two cell lines that show different resistance to ROS mediated toxicity.

The higher resistance of A549 cells to AgNPs may be due to their higher expression of protective genes coding for antioxidant and detoxifying enzymes, as already shown for different nanoparticles in a previous work by our group.[29]

As shown in Figure 2, the silver ion release from AgNPs in culture medium conditions is rather weak (and much lower than in lysosomes). Moreover, most of the free silver ions in complete serum cell culture medium are chelated by proteins[55] or precipitate as insoluble silver salts (e.g., AgCl or Ag_3PO_4), reducing the silver ions toxicity.[56] This observation emphasizes by itself the role of internally derived ions as main cause of ROS and subsequent cytotoxicity.

With the present work we definitively show that AgNP toxicity is mainly dependent on the presence of Ag^+ ions inside cell cytosol. In particular, the ions are released from AgNPs previously internalized by the cell through the endocytosis pathway, driving the particles to the lysosomes. The acidic environment of the final-fate endocytosis' organelles leads to nanoparticle dissolution with release of ions, which are subsequently found in the cytosol. Hence, the cytotoxicity induced by the presence of AgNPs, leading to oxidative stress, DNA damage and cell death, is mainly due to the impairment of physiological metabolic and cell cycle mechanism by intracellular silver ions. We demonstrated this hypothesis by a complete set of analysis in different cell types and experimental conditions. The possibility to prevent AgNP-induced cytotoxicity using Ag^+ chelating agents ultimately demonstrates the cell death mechanism.

It should be taken in consideration that, above a certain dose of Ag^+ ions in the medium, cell death is inevitable, as shown in Figure 4 and reported in literature.[43,57] At ion concentrations ≥ 5 μg/ml, HeLa cells die within few hours, due to membrane permeability impairment by extracellular Ag^+ ions interacting with sulphydryl groups of cell membrane proteins.[44] This membrane mechanism is independent of intracellular accumulation of silver ions, unlike in the case of AgNPs.

Nevertheless, we must emphasize the importance of the different syntheses of AgNPs that determine their physical/chemical properties (size, shape, surface charge and chemistry), which, in turn, affect their dissolution in specific media.[3] Such features, together with the biological models used (e.g., eukariotic or prokariotic cells), are the main cause of some discrepancies.[58-62]

Further research should be performed *in vivo* to confirm the mechanisms and to gain a comprehensive picture of AgNP-induced toxicity in mammals. This may greatly help the material science community to develop safer nanoparticles and regulatory bodies to establish proper guidelines and directives of AgNPs.

References

1. Wang A, Marinakos SM, Badireddy AR, Powers CM, Houck K. Characterization of physicochemical properties of nanomaterials and their immediate environments in high-throughput screening of nanomaterial biological activity. Wires Nanomed Nanobiotechnol 2013;5:430-48.

2. Chen X, Schluesener HJ. Nanosilver: a nanoproduct in medical application. Toxicol Lett 2008;176:1-12.

3. Rizzello L, Pompa PP. Nanosilver-based antibacterial drugs and devices: mechanisms, methodological drawbacks, and guidelines. Chem Soc Rev 2014;43:1501-18.

4. Chaudhry Q, Scotter M, Blackburn J, Ross B, Boxall A, Castle L, et al. Applications and implications of nanotechnologies for the food sector. Food Addit Contam Part A 2008;25:241-58.

5. Ahamed M, AlSalhi MS, Siddiqui MKJ. Silver nanoparticle applications and human health. Clin Chim Acta 2010;411:1841-8.

6. Benn TM, Westerhoff P. Nanoparticle silver released into water from commercially available sock fabrics. Environ Sci Technol 2008;42:4133-9.

7. Fan M, Thompson M, Andrade ML, Brolo AG. Silver nanoparticles on a plastic platform for localized surface plasmon resonance biosensing. Anal Chem 2010;82:6350-2.

8. Zhang ZL, Zhang XY, Xin ZQ, Deng MM, Wen YQ, Song YL. Synthesis of monodisperse silver nanoparticles for ink-jet printed flexible electronics. Nanotechnology 2011;22, http://dx.doi.org/10.1088/0957-4484/22/42/425601.

9. Son Y, Yeo J, Moon H, Lim TW, Hong S, Nam KH, et al. Nanoscale electronics: digital fabrication by direct femtosecond laser processing of metal nanoparticles. Adv Mater 2011;23:3176-81.

10. Kim TH, Kim M, Park HS, Shin US, Gong MS, Kim HW. Size-dependent cellular toxicity of silver nanoparticles. J Biomed Mater Res A 2012;100A:1033-43.

11. Lim DH, Jang J, Kim S, Kang T, Lee K, Choi IH. The effects of sub-lethal concentrations of silver nanoparticles on inflammatory and stress genes in human macrophages using cDNA microarray analysis. Biomaterials 2012;33:4690-9.

12. Haase A, Rott S, Mantion A, Graf P, Plendl J, Thunemann AF, et al. Effects of silver nanoparticles on primary mixed neural cell cultures: uptake, oxidative stress and acute calcium responses. Toxicol Sci 2012;126:457-68. Greulich C, Diendorf J, Simon T, Eggeler G, Epple M, Koller M. Uptake and intracellular distribution of silver nanoparticles in human mesenchymal stem cells. Acta Biomater 2012;7:347-54.

13. Van der Zande M, Vandebriel RJ, Van Doren E, Kramer E, Rivera ZH, Serrano-Rojero CS, et al. Distribution, elimination, and toxicity of silver nanoparticles and silver ions in rats after 28-day oral exposure. ACS Nano 2012;6:7427-42.

14. Rahman MF,Wang J, Patterson TA, Saini UT, Robinson BL, Newport GD, et al. Expression of genes related to oxidative stress in the mouse brain after exposure to silver-25 nanoparticles. Toxicol Lett 2009;187:15-21.

15. Lim D, Roh JY, Eom HJ, Choi JY, Hyun J, Choi J. Oxidative stress-related PMK-1 P38 MAPK activation as a mechanism for toxicity of silver nanoparticles to reproduction in the nematode Caenorhabditis elegans. Environ Toxicol Chem 2012;31:585-92.

16. Roh JY, Sim SJ, Yi J, Park K, Chung KH, Ryu DY, et al. Ecotoxicity of silver nanoparticles on the soil nematode Caenorhabditis elegans using functional ecotoxicogenomics. Environ Sci Technol 2009;43:3933-40.

17. Choi JE, Kim S, Ahn JH, Youn P, Kang JS, Park K, et al. Induction of oxidative stress and apoptosis by silver nanoparticles in the liver of adult zebrafish. Aquat Toxicol 2010;100:151-9.

18. Bilberg K, Malte H, Wang T, Baatrup E. Silver nanoparticles and silver nitrate cause respiratory stress in Eurasian perch (Perca fluviatilis). Aquat Toxicol 2010;96:159-65.

19. Panacek A, Prucek R, Safarova D, Dittrich M, Richtrova J, Benickova K, et al. Acute and chronic toxicity effects of silver nanoparticles (NPs) on Drosophila melanogaster. Environ Sci Technol 2011;45:4974-9.

20. Hansen SF, Baun A. When enough is enough. Nat Nanotechnol 2012;7:409-11.

21. Yen HJ, Hsu SH, Tsai CL. Cytotoxicity and immunological response of gold and silver nanoparticles of different sizes. Small 2009;5:1553-61.

22. Sur I, Altunbek M, Kahraman M, Culha M. The influence of the surface chemistry of silver nanoparticles on cell death. Nanotechnology 2012;23, http://dx.doi.org/10.1088/0957-4484/23/37/375102.

23. Wijnhoven SWP, Peijnenburg WJGM, Herberts CA, Hagens WI, Oomen AG, Heugens EHW, et al. Nano-silver—a review of available data and knowledge gaps in human and environmental risk assessment. Nanotoxicology 2009;3:109-38.

24. Kim S, Choi JE, Choi J, Chung KH, Park K, Yi J, et al. Oxidative stressdependent toxicity of silver nanoparticles in human hepatoma cells. Toxicol in Vitro 2009;23:1076-84.

25. Kawata K, Osawa M, Okabe S. In vitro toxicity of silver nanoparticles at noncytotoxic doses to HepG2 human hepatoma cells. Environ Sci Technol 2009;43:6046-51.

26. Park EJ, Yi J, Kim Y, Choi K, Park K. Silver nanoparticles induce cytotoxicity by a Trojan-horse type mechanism. Toxicol in Vitro 2010;24:872-8.

27. Dadosh T. Synthesis of uniform silver nanoparticles with a controllable size. Mater Lett 2009;63:2236-8.

28. Malvindi MA, Brunetti V, Vecchio G, Galeone A, Cingolani R, Pompa PP.

SiO2 nanoparticles biocompatibility and their potential for gene delivery and silencing. Nanoscale 2012;4:486-95.

29. Brunetti V, Chibli H, Fiammengo R, Galeone A, Malvindi MA, Vecchio G, et al. InP/ZnS as a safer alternative to CdSe/ZnS core/shell quantum dots: in vitro and in vivo toxicity assessment. Nanoscale 2013;5:307-17.

30. Maiorano G, Sabella S, Sorce B, Brunetti V, Malvindi MA, Cingolani R, et al. Effects of cell culture media on the dynamic formation of protein-nanoparticle complexes and influence on the cellular response. ACS Nano 2010;4:7481-91.

31. Malvindi MA, De Matteis V, Galeone A, Brunetti V, Anyfantis GC, Athanassiou A, et al. Toxicity assessment of silica coated iron oxide nanoparticles and biocompatibility improvement by surface engineering. PLoS One 2014;9, http://dx.doi.org/10.1371/journal.pone.0085835.

32. Hsin YH, Chena CF, Huang S, Shih TS, Lai PS, Chueh PJ. The apoptotic effect of nanosilver is mediated by a ROS- and JNK-dependent mechanism involving the mitochondrial pathway in NIH3T3 cells. Toxicol Lett 2008;179:130-9.

33. Teodoro JS, Simoes AM, Duarte FV, Rolo AP, Murdoch RC, Hussain SM, et al. Assessment of the toxicity of silver nanoparticles in vitro: a mitochondrial perspective. Toxicol in Vitro 2011;25:664-70.

34. Hackenberg S, Scherzed A, Kessler M, Hummel S, Technau A, Froelich K, et al. Silver nanoparticles: evaluation of DNA damage, toxicity and functional impairment in human mesenchymal stem cells. Toxicol Lett 2011;201:27-33.

35. Eom HJ, Choi J. p38 MAPK activation, DNA damage, cell cycle arrest and apoptosis as mechanisms of toxicity of silver nanoparticles in Jurkat T cells. Environ Sci Technol 2010;44:8337-42.

36. Pellegata NS, Antoniono RJ, Redpath JL, Stanbridge EJ. DNA damage and p53-mediated cell cycle arrest: a reevaluation. Proc Natl Acad Sci U S A 1996;93:15209-14.

37. Boonstra J, Post JA. Molecular events associated with reactive oxygen species and cell cycle progression in mammalian cells. Gene 2004;337:1-13.

38. AshaRani PV, Mun GLK, Hande MP, Valiyaveettil S. Cytotoxicity and genotoxicity of silver nanoparticles in human cells. ACS Nano 2009;3:279-90.

39. Porter AG, Janicke RU. Emerging roles of caspase-3 in apoptosis. Cell Death Differ 1999;6:99-104.

40. Nicholson DW, Ali A, Thornberry NA, Vaillancourt JP, Ding CK, Gallant M, et al. Identification and inhibition of the ICE/CED-3 protease necessary for mammalian apoptosis. Nature 1995;376:37-43.

41. Hu MM, Fan JL, Cao JF, Song KD, Zhang H, Sun SG, et al. Enhanced fluorescent chemosensor for Ag+ in absolute aqueous solution and living cells: an experimental and theoretical study. Analyst 2012;137:2107-11.

42. Reidy B, Haase A, Luch A, Dawson KA, Lynch I. Mechanisms of silver nanoparticle release, transformation and toxicity: a critical review of

738 V. De Matteis et al / Nanomedicine: Nanotechnology, Biology, and Medicine 11 (2015) 731–739current knowledge and recommendations for future studies and applications. Materials 2013;6:2295-350.

43. Beer C, Foldbjerg R, Hayashi Y, Sutherland DS, Autrup H. Toxicity of silver nanoparticles—nanoparticle or silver ion? Toxicol Lett 2012;208:286-92.

44. Kone BC, Kaleta M, Gullans SR. Silver ion (Ag+)-induced increases in cell membrane K+ and Na+ permeability in the renal proximal tubule: reversal by thiol reagents. J Membr Biol 1988;102:11-9.

45. Sigel A, Sigel H, Sigel RKO. Metallothioneins and related chelators. Metal ions in life sciences, vol. 5. Cambridge, England: Royal Society of Chemistry1-84755-899-2; 2009. p. 44.

46. Nordberg M, Nordberg GF. Metallothioneins: historical development and overview. Metal ions in life sciences, 5. Cambridge, England: Royal Society of Chemistry1-84755-899-2; 2009. p. 1-29.

47. Luther EM, Schmidt MM, Diendorf J, Epple M, Dringen R. Upregulation of metallothioneins after exposure of cultured primary astrocytes to silver nanoparticles. Neurochem Res 2012;37:1639-48.

48. Park EJ, Bae E, Yi J, Kim Y, Choi K, Lee SH, et al. Repeated-dose toxicity and inflammatory responses in mice by oral administration of silver nanoparticles. Environ Toxicol Pharmacol 2010;30:162-8.

49. Vecchio G, Fenech M, Pompa PP, Voelcker NH. Lab-on-a-chip-based high-throughput screening of the genotoxicity of engineered nanomaterials. Small 2014;10:2721-34, http://dx.doi.org/10.1002/smll.201303359.

50. Kim S, Ryu DY. Silver nanoparticle-induced oxidative stress, genotoxicity and apoptosis in cultured cells and animal tissues. J Appl Toxicol 2013;33:78-89.

51. Franco R, Sanchez-Olea R, Reyes-Reyes EM, Panayiotidis MI. Environmental toxicity, oxidative stress and apoptosis: menage a trois. Mutat Res 2009;674:3-22.

52. Carlson C, Hussain SM, Schrand AM, Braydich-Stolle LK, Hess KL, Jones RL, et al. Unique cellular interaction of silver nanoparticles: size-dependent generation of reactive oxygen species. J Phys Chem B 2008;112:13608-19.

53. Ahamed M, Karns M, Goodson M, Rowe J, Hussain SM, Schlager JJ, et al. DNA damage response to different surface chemistry of silver nanoparticles in mammalian cells. Toxicol Appl Pharmacol 2008;233:404-10.

54. Piao MJ, Kang KA, Lee IK, Kim HS, Kim S, Choi JY, et al. Silver nanoparticles induce oxidative cell damage in human liver cells through inhibition of reduced glutathione and induction of mitochondriainvolved apoptosis. Toxicol Lett 2011;201:92-100.

55. Ostermeyer AK, Mumuper CK, Semprini L, Radniecki T. Influence of bovine serum albumin and alginate on silver nanoparticle dissolution and toxicity to Nitrosomonas europaea. Environ Sci Technol 2013;47:14403-10.

56. Liu JY, Sonshine DA, Shervani S, Hurt RH. Controlled release of biologically active silver from nanosilver surfaces. ACS Nano 2010;4:6903-13.

57. Pratsinis A, Hervella P, Leroux JC, Pratsinis SE, Sotiriou GA. Toxicity of silver nanoparticles in macrophages. Small 2013;9:2576-84.

58. Loza K, Diendorf J, Sengstock C, Ruiz-Gonzalez L, Gonzalez-Calbet JM, Vallet-Regi M, Köller M, Epple M. The dissolution and biological effects of silver nanoparticles in biological media. J Mater Chem B 2014;2:1634-43.

59. Zhang W, Yao Y, Sullivan N, Chen Y. Modeling the primary size effects of citrate-coated silver nanoparticles on their ion release kinetics. Environ Sci Technol 2011;45:4422-8.

60. Liu J, Hurt RH. Ion release kinetics and particle persistence in aqueous nano-silver colloids. Environ Sci Technol 2010;44:2169-75.

61. Gliga AR, Skoglund S, Wallinder IO, Fadeel B, Karlsson HL. Sizedependent cytotoxicity of silver nanoparticles in human lung cells: the role of cellular uptake, agglomeration and Ag release. Part Fibre Toxicol 2014;11:11.

62. Bondarenko O, Ivask A, Käkinen A, Kurvet I, Kahru A. Particle-cell contact enhances antibacterial activity of silver nanoparticles. PLoS One 2013;8(5):e64060.

SUPPORTING INFORMATION

Methods and materials

Dynamic Light Scattering (DLS) and ζ-Potential Measurements

Dynamic Light Scattering (DLS) and ζ-Potential measurements were performed on a Zetasizer Nano ZS90 (Malvern, USA). Measurements were made at 25 °C in aqueous solutions (pH 7) and in cell culture medium. Cell culture medium DMEM high glucose (Sigma) was supplemented with 10% of Fetal Bovine Serum (FBS) (Gibco Invitrogen), with 50 μM glutamine (Gibco), 1 mM sodium pyruvate (Gibco) 100 U/mL penicillin and 100 mg/mL streptomycin (Invitrogen). Measurements were also taken after 96 h of incubation.

Nanoparticle tracking analysis (NTA)

Nanoparticle tracking analysis (NTA) measurements were performed on a NanoSight NS500 (Nanosight, United Kingdom). Measurements were made at 25 °C in water and complete cell at the final concentration of 2.5×106 nanoparticles/mL. Measurements were also taken after 96 h of incubation.

UV-vis measurements

The optical absorbance spectra of AgNPs were measured with a Cary 300 UV–vis spectrophotometer at a resolution of 1 nm using a 5 mm path length quartz cuvettes. Measurements were made both in aqueous solutions (pH = 7) and in cell culture medium also after 96 h of incubation.

Confocal Microscopy Imaging

For internalization and colocalization of AgNPs with lysosomes, AgNPs were excited at 570 nm in scattering mode (the emission was acquired in the spectral window at 567-573 nm). Lysosomes were imaged by exciting the LysoTracker Red DND-99 with the 577 nm line of the white light laser (WLL, Leica), and acquired in the emission range of 600–680 nm.

TEM analyses

Transmission electron microscope (TEM) images of AgNPs were recorded by a JEOL Jem 1011 microscope operating at an accelerating voltage of 100 kV. TEM samples were prepared by dropping a dilute solution of nanoparticles in water on carbon-coated copper grids (Formvar/Carbon 300 Mesh Cu). For cell imaging, AgNPs-treated cells were thoroughly washed with PBS buffer and scraped from the culture dish, and then centrifuged at 300g for 5 min. The cell pellets were fixed

in PBS solution containing 2.5% gluteraldehyde and 4% paraformaldehyde for 1 h. They were then rinsed with PBS, embedded in 2% agarose gel. Gel embedded cells were automatically processed in Automatic Microwave Tissue Processor for Electron Microscopy (Leica EM AMW) following a standard protocol for soft tissues: post-fixation in 1% osmium tetroxyde in PBS, dehydratation in graded series of ethanol/acetone, and epoxy resin infiltration and embedding (45% epon812, 30% DDSA, 23% MNA, 2% DMP30). Ultrathin sections (70 nm) were obtained with a Leica EM UC7 ultramicrotome, deposited onto carbon-coated copper grids (Formvar/Carbon 300 Mesh Cu), and then stained with 5% aqueous uranyl acetate and 2% aqueous lead citrate, by using Leica EM AC20. Cells were finally imaged with a JEOL Jem 1011 TEM.

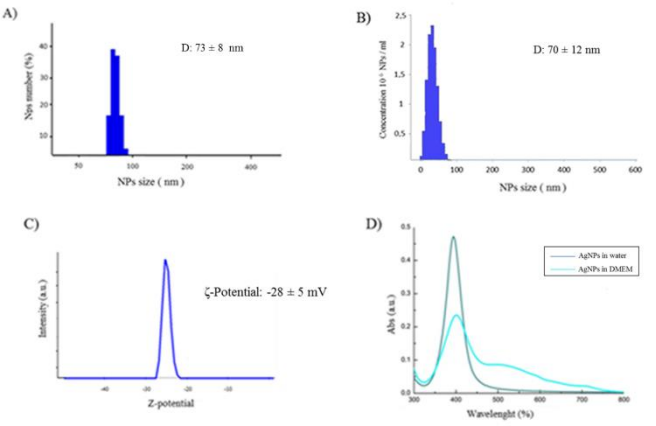

Figure S1. Characterization of silver nanoparticles (AgNPs) in water. A) Representative TEM image and size distribution; B) Dynamic light scattering (DLS); C) Nanoparticle tracking analysis (NTA); D) ζ-Potential measurement; E) UV-vis spectrum. **Figure S2.** Characterization of AgNPs after 96 h incubation in cell culture medium (DMEM). A) Dynamic light scattering; B) Nanoparticle tracking analysis (NTA); C) ζ-potential measurements; D) UV-vis spectra.

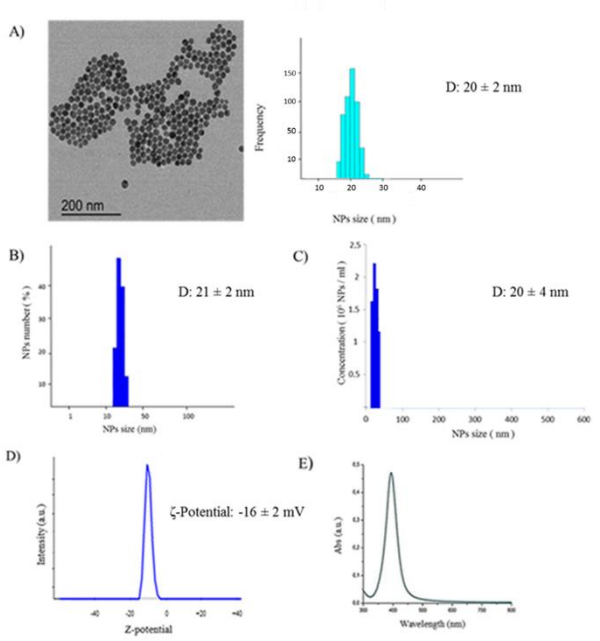

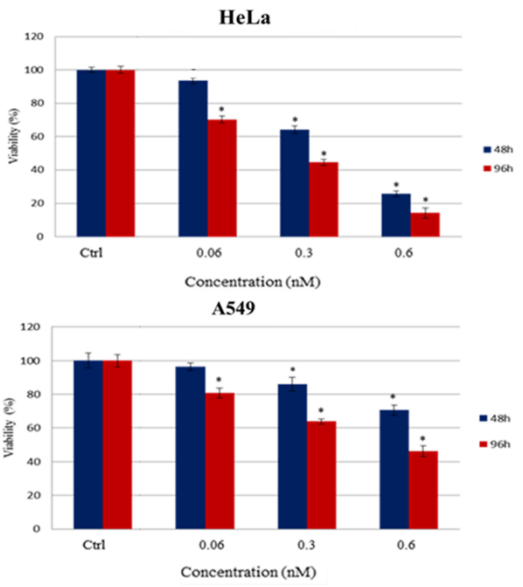

1.

2. **Figure S3.** Viability assay (WST-8) of HeLa and A549 cells after 48 and 96 h exposure to increasing doses of AgNPs (nanoparticle concentrations of 0.06, 0.3, 0.6 nM). Percent viability of nanoparticle-treated cells is expressed relative to non-treated control cells. As positive control (P), cells were incubated with 5% DMSO showing a ca. 60% viability decrease (not shown). Data are reported as mean ±SD from three independent experiments; *P < 0.05 compared with control (n= 8).

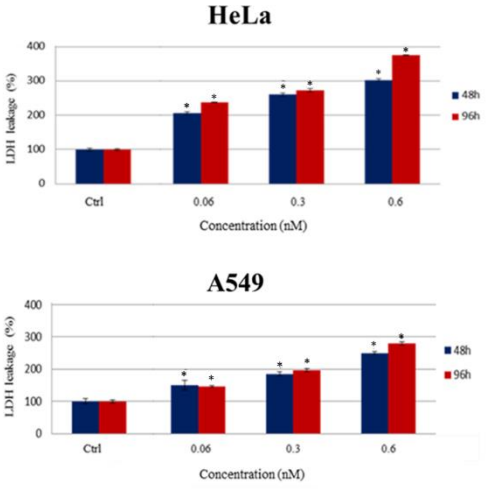

Figure S4. LDH assay on HeLa and A549 cells incubated with increasing concentrations (nanoparticle concentrations of 0.06, 0.3, and 0.6 nM) of AgNPs at different times (48 and 96 h). Percent of LDH leakage of nanoparticle-treated cells are expressed relative to non-treated control cells. Positive controls (P) consisted in the treatment of cells with 0.9% Triton X-100 showing ca. 500 % LDH increase (not shown). Data are reported as mean ± SD from three independent experiments; *P < 0.05 compared with control (n= 8).

3.

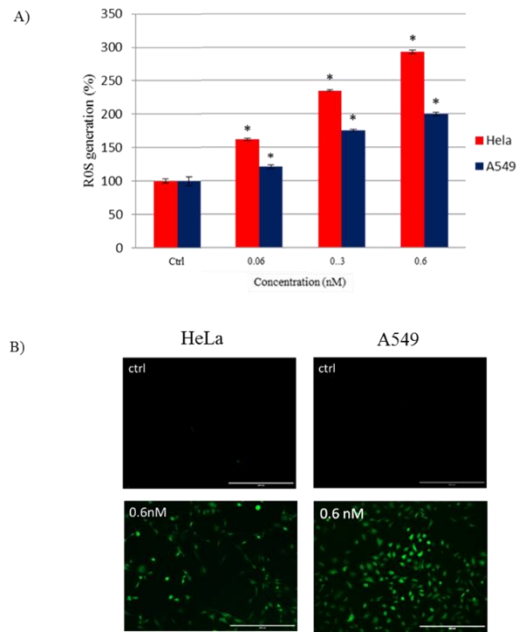

Figure S5. A) Effect of AgNPs on the ROS level in HeLa and A549 cells. Cells were treated with different concentrations of AgNPs (nanoparticle concentrations of 0.06, 0.3, 0.6 nM) for 48 h, incubated with 100 µM DCFH-DA, then washed with PBS buffer, and the fluorescence of the cells from each well was measured and recorded. ROS generation of nanoparticle-treated cells is expressed relative to non-treated control cells. As a positive control (P), cells were incubated with 500 µM H_2O_2 showing a ca. 300 % DCFH-DA increase (not shown). Data are reported as mean ±SD from three independent experiments; *P<0.05 compared with control (n= 8). B) Representative fluorescence images of HeLa and A549 cells treated for 48 h with 0.6 nM AgNPs and incubated with DCFH-DA (100 µM).

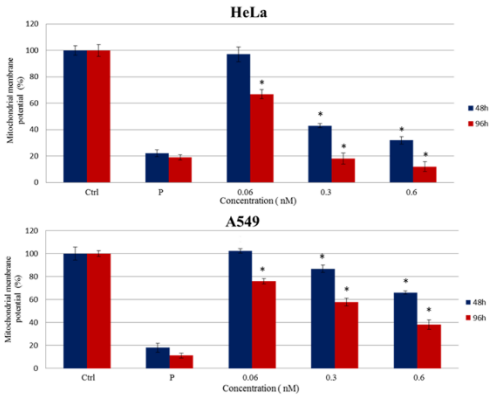

Figure S6. Effect of AgNPs on mitochondrial membrane potential (MMP) in HeLa and A549 cells. Cells were treated with increasing concentrations of NPs **Figure S8**. Effect of AgNPs on levels of apoptosis. Caspase-3 assay was performed incubating A549 and HeLa cells with 0.6 nM AgNPs for 24 h. Data are reported as mean ±SD from three independent experiments; *P<0.05 compared with (nanoparticle concentrations of 0.06, 0.3, and 0.6 nM) for 48 and 96 h, incubated with 2.5 µg/mL of JC1, washed with PBS buffer, and the fluorescence of the cells from each well was measured and recorded. Percent mitochondrial membrane potential of nanoparticle-treated cells is expressed relative to non-treated control cells. As a positive control (P), cells were incubated with 100 µM valinomycin. Data are reported as mean ±SD from three independent experiments;

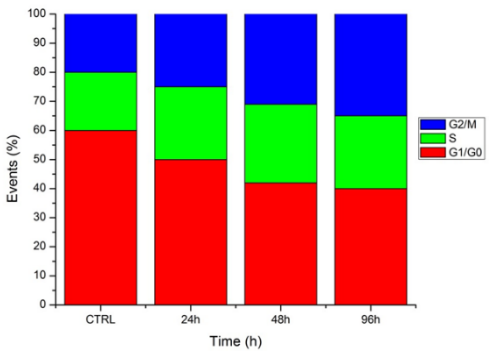

Figure S7. Effect of AgNPs on HeLa cell cycle. HeLa cells were treated with a concentration 0.6 nM of AgNPs for 3 h, and the cell cycle was detected after 24, 48 and 96 h. Cell cycle statistic was determined by flow cytometry analysis.

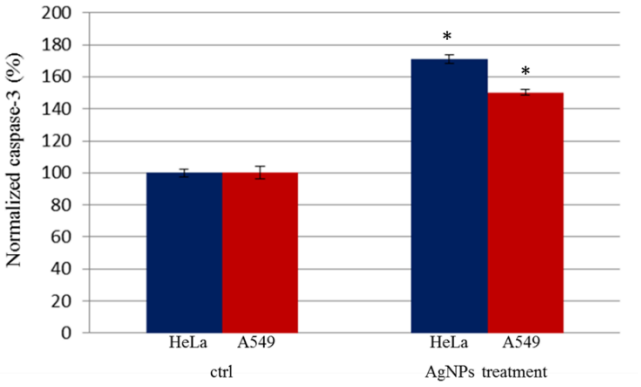

Figure S8. Effect of AgNPs on levels of apoptosis. Caspase-3 assay was performed incubating A549 and HeLa cells with 0.6 nM AgNPs for 24 h. Data are reported as mean ±SD from three independent experiments; *P<0.05 compared with control (n= 8).
control (n= 8).
*P<0.05 compared with control (n= 8)

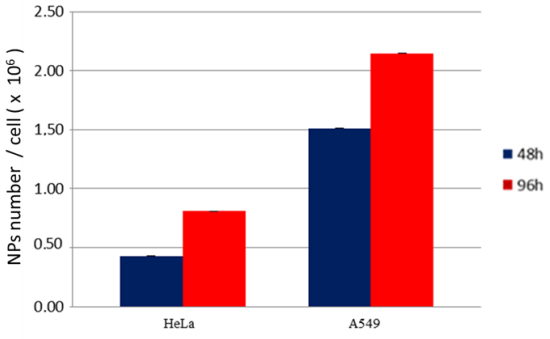

Figure S9. Internalization data for HeLa and A549 cells expressed as the number of internalized AgNPs (determined by ICP-AES) per cell after 48 and 96 h of NPs incubation (at 0.6 nM). In these experiments, we extensively washed the cells before ICP measurements, in order to remove non-internalized, membrane-bound NPs. Such procedure allowed us to remove most of non-internalized particles, as also assessed by confocal microscopy imaging (Fig. S10). However, a small error, due to adherent NPs on the cell surface, can be present in the data reported here, not affecting the general conclusions.

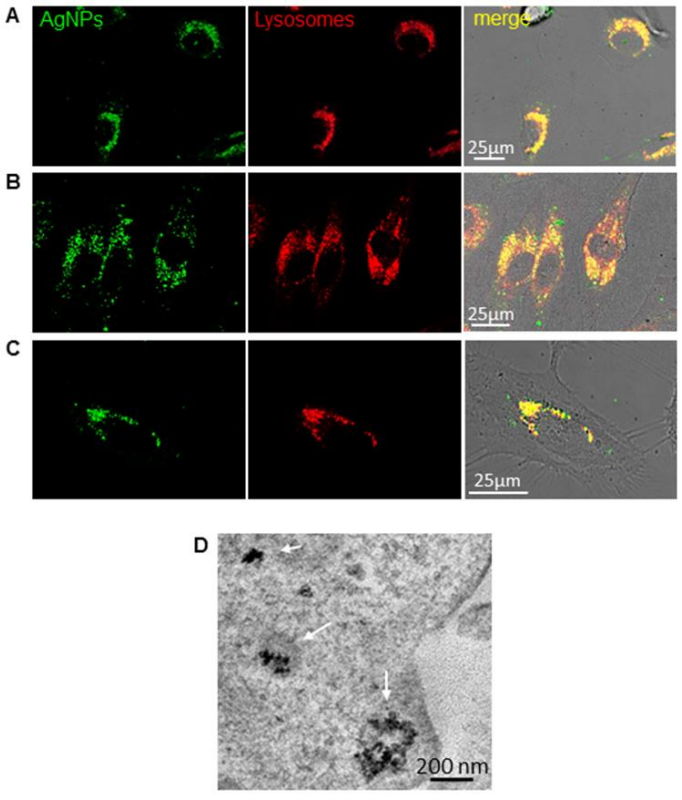

Figure S10. AgNPs colocalize with lysosomes. (A-C) Cellular uptake of AgNPs visualized by confocal microscopy imaging in living cells. Three representative confocal images of HeLa cells incubated for 48 hours with 0.6 nM AgNPs. AgNPs are shown in green, lysosomes are stained with Lysotracker Red probe. Note in the merged images the colocalization (yellow) of AgNPs within the lysosomes. (D) Representative TEM image of AgNP uptake in HeLa cells. Note the accumulation of the nanoparticles in the intracellular vesicles (white arrows).

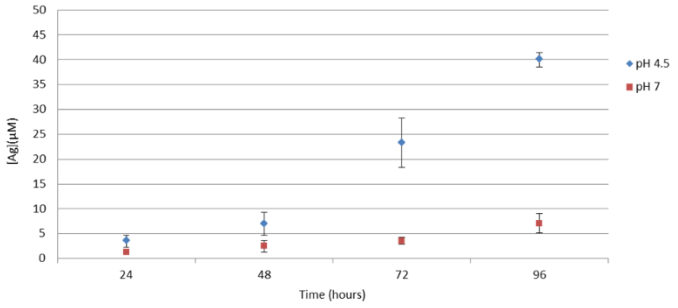

Figure S11. Effects of time and pH on silver ions release from AgNPs (10 nM). NPs degradation was evaluated both at pH 4.5 and 7 up to 96 h. NPs degradation in neutral conditions was analyzed also in culture medium, finding the same behavior observed in water.